Dimorphism throughout the European eel's life cycle: are ontogenetic changes in head shape related to dietary differences?

J. De Meyer,[1] T. Goethals,[1] S. Van Wassenbergh,[1,2] T. Augustijns,[1] J. Habraken,[1] J. Hellemans,[1] V. Vandewiele,[1] J. Dhaene,[3] M. Bouillart[1] and D. Adriaens[1]

[1]*Evolutionary Morphology of Vertebrates, Ghent University, Ghent, Belgium*
[2]*Département Adaptations du Vivant, UMR 7179 C.N.R.S/M.N.H.N., Paris Cedex 05, France*
[3]*Department of Physics and Astronomy, UGCT – Radiation Physics, Ghent University, Ghent, Belgium*

Abstract

A well-known link exists between an organism's ecology and morphology. In the European eel, a dimorphic head has been linked to differences in feeding ecology, with broad-headed eels consuming harder prey items than narrow-headed ones. Consequently, we hypothesized that broad-heads should exhibit a cranial musculoskeletal system that increases bite force and facilitates the consumption of harder prey. Using 3D-reconstructions and a bite model, we tested this hypothesis in two life stages: the sub-adult yellow eel stage and its predecessor, the elver eel stage. This allowed us to test whether broad- and narrow-headed phenotypes show similar trait differences in both life stages and whether the dimorphism becomes more pronounced during ontogeny. We show that broad-headed eels in both stages have larger jaw muscles and a taller coronoid, which are associated with higher bite forces. This increased bite force together with the elongated upper and lower jaws in broad-headed eels can also improve grip during spinning behavior, which is used to manipulate hard prey. Head shape variation in European eel is therefore associated with musculoskeletal variation that can be linked to feeding ecology. However, although differences in muscle volume become more pronounced during ontogeny, this was not the case for skeletal features.

Key words: anguilliformes; bite force; cranial osteology; feeding; myology.

Introduction

Many aspects of an organism's ecology can be predicted from studying its morphology and vice versa, with feeding ecology of particular interest. Morphological variation in the feeding apparatus can lead to differences in feeding performance among individuals of the same species and/or among co-existing species, subsequently resulting in differences in resource use (Arnold, 1983). The relation between feeding ecology and the morphology of the feeding apparatus has therefore been extensively studied and is nowadays well established (Saunders & Barclay, 1992; Norton & Brainerd, 1993; Hahn & Cunha, 2005; Narayani et al. 2015; Iijama, 2017). For example, Midas cichlids develop molariform lower pharyngeal jaws in response to hard prey, whereas papilliform jaws are developed in individuals

eating soft prey items (Meyer, 1989). Perciform fish feeding on teleosts exhibit a high width–height aspect ratio and symmetrical, caudally expanded dorsal and pectoral fins, allowing an extensive control of the attack angle and enhanced maneuverability. By contrast, perciforms feeding on crustaceans such as shrimp, display a more streamlined body, maximizing thrust and allowing high amplitude propulsion movements to capture such prey effectively (Webb, 1984; Bohórquez-Herrera et al. 2014).

However, all these studies focus on individuals of the same age, whereas other studies have shown that diets can shift during ontogeny. Espinoza et al. (2012) showed that immature rasptail skate (*Raja velezi* Chirichigno, 1973) and brown smoothhound shark (*Mustelus henlei* Gill, 1863) mainly consume crustaceans, but switched to teleosts when mature. The same change in diet is observed in goliath groupers (Artero et al. 2015). Although not switching from a crustacean to a teleost diet, European anchovies and pilchards (Costalago et al. 2012) and Commerson's dolphins (Riccialdelli et al. 2013) are also known to undergo a dietary shift during ontogeny. These studies indicate that to understand fully a species' ecomorphology, it is necessary to study

its morphology and ecology during its complete life cycle. Although the list of ecomorphological studies is extensive, only a few studies have focused on morphological changes related to species-specific dietary shifts as individuals grow (Hernandez & Motta, 1997; Herrel & O'Reilly, 2006; Machado-Evangelista et al. 2015; Santana & Miller, 2016; Wilga et al. 2016).

In the European eel (*Anguilla anguilla* Linnaeus, 1758), such ontogenetic dietary shifts also occur. First, eels prefer prey items suited to their body size (Tesch, 2003). As such, the longer and larger an eel becomes, the larger prey items it can consume. Small eels (10–30 cm body length) mainly feed on insect larvae such as Trichoptera larvae, chironomids and small crustaceans, whereas the stomachs of eels of 20–40 cm also contain larger crustaceans and molluscs (Sinha & Jones, 1967). When the eels become even larger, the proportion of fish increases in their diet (Moriarty, 1973). However, the type of prey is not only correlated with body size but is also linked to head shape. Head shape is dimorphic in the sub-adult yellow eels, with more extreme broad- and narrow-headed eels being present in a single population compared with eels with an intermediate head shape (Ide et al. 2011). Broad-headed yellow eels are characterized by both a broader general head width and also a wider mouth (Thurow, 1958 Lammens & Visser, 1989; Proman & Reynolds, 2000; Ide et al. 2011; De Meyer et al. 2016). Their diet mainly consists of harder prey items, such as large crustaceans and fish, whereas that of narrow-headed phenotypes generally includes small invertebrates such as insect larvae. However, the yellow eel stage (pigmentation stage VII according to Bertin, 1956; fully pigmented) is preceded by the leptocephalus stage, glass eel stage and elver eel stage (Fig. 1). After crossing the ocean as feeding leptocephalus larvae, they undergo a metamorphosis to unpigmented glass eels. These glass eels are non-feeding in the initial pigmentation stages (Va and Vb according to Bertin, 1956; characterized by no pigment except for the tip of the tail and the head at the height of the skull). In a previous study, De Meyer et al. (2015) showed that there was a range of broad- and narrow-headed phenotypes already present in these non-feeding stages. However, since many glass eels with an intermediate head shape were still present, the head shape variation did not follow a bimodal distribution in glass eels. Feeding in the eels starts simultaneously with the start of pigmentation, when the eels reach the elver eel stage (pigmentation stage VIa–VIb according to Bertin, 1956; characterized by the development of pigmentation along the whole dorsum, increased pre- and post-anal pigmentation and pigment rows along the myosepta). In another study, De Meyer et al. (2016) showed that dietary differences in the latter stage can stimulate the development of more extreme broad and narrow heads, with eels still being smaller than 15 cm.

Since variation in head shape is likely related to diet, it should be associated to musculoskeletal variation as well.
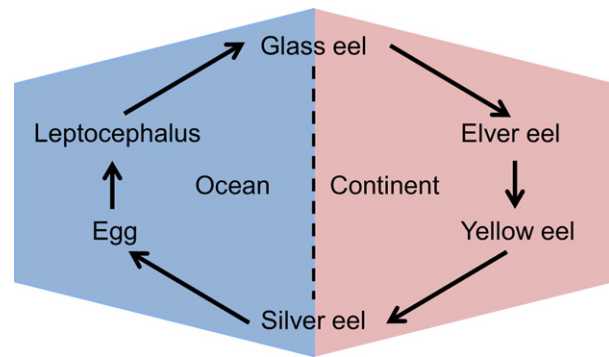

Fig. 1 Diagram showing the different stages of the European eel life cycle.

Indeed, a recent study on glass eels indicated that broad-headed glass eels exhibit larger jaw muscles, a longer lower jaw with a heightened coronoid, and a broader skull as compared with narrow-headed glass eels (De Meyer et al. 2018). These features are associated with higher bite forces and facilitate the consumption of harder prey (De Meyer et al. 2018). By comparing the musculoskeletal morphology between broad- and narrow-headed phenotypes in the subsequent life stages (elver and yellow eel stage), we wanted to identify the musculoskeletal features characterizing both phenotypes in each life stage. As mentioned above, larger eels can also consume larger prey. Consequently, larger eels should have a broader diet than smaller ones and the largest differences in consumed prey items could be expected in the yellow eel stage. Accordingly, we wanted to test whether differences in musculoskeletal morphology between broad- and narrow-heads become more pronounced with age, eventually leading to the dimorphism observed in yellow eels.

Additionally, as previous studies already showed that head size and bite force are related (Verwaijen et al. 2002; Marshall et al. 2012), we linked the observed musculoskeletal variation to bite force using a bite model. Bite force is an excellent measure of ecological performance related to prey capture and processing (Wainwright & Reilly, 1994; Herrel et al. 2001b). Differences in bite force have been related to dietary diversity (Wainwright, 1988; Clifton & Motta, 1998), niche diversification (Herrel et al. 2001a; Lopez-Darias et al. 2015) and ontogenetic dietary shifts (Hernandez & Motta, 1997; Wyckmans et al. 2007). In all cases, resource utilization was limited by the generated bite forces. As we expected that musculoskeletal variation could increase during ontogeny, we also expected larger differences in bite force between broad- and narrow-heads in the yellow eel stage than in the elver eel stage, which then can be linked to the consumed prey. In this study, we thus compared both morphology and performance between different phenotypes within one life stage, and also between different life stages.

Materials and methods

Sample collection

Taking total body length into consideration, five of the most broad-headed (BH) and five of the most narrow-headed (NH) elver eels were selected from a sample previously used to perform a shape analysis (De Meyer et al. 2016) and were used for μCT-scanning (Fig. 2, Supporting Information Table S1). As described in more detail in the paper by De Meyer et al. (2016), four of these broad-heads were fed a hard diet that required biting and spinning behavior (hard feeders). During spinning behavior, eels grab prey items with their mouth and spin along their long axis, tearing off smaller prey items (Helfman & Winkelman, 1991). Three of the five narrow-heads were given soft prey that only required suction feeding (soft feeders). Additionally, one extra broad-headed and two extra narrow-headed elvers were selected that received a mixture of both diets (control feeders). Head width of these specimens was

measured just posterior to the eye and the head width/total length ratio (HW/TL) was calculated to confirm the results of the shape analysis (mean HW/TL ± SD: 0.0356 ± 0.0034 for BH; 0.0290 ± 0.0025 for NH). For the yellow eels, a sample was collected in the river Demer (n = 31; Belgium). The head shape of the used elver eels was induced by feeding them strict diets, but the yellow eels were caught in the wild and these could consequently have had a less specialized diet. All eels were anesthetized with MS222 and killed by an MS222-overdose, in accordance with Belgian legislation. Broad- and narrow-headed yellow eels were selected based on HW/TL. Specimens with HW/TL above 0.036 are considered broad-heads and specimens with a HW/TL lower than 0.030 are considered narrow-heads. Using these criteria, five eels were broad-headed and 16 eels were narrow-headed, with the remaining 10 eels being considered intermediate. The higher number of intermediates than broad-heads is due to the low sample size. Of these eels, three narrow- and broad-heads each were also μCT-scanned (Table S1). The total length of the eels was measured to the nearest 0.1 mm. Sex of
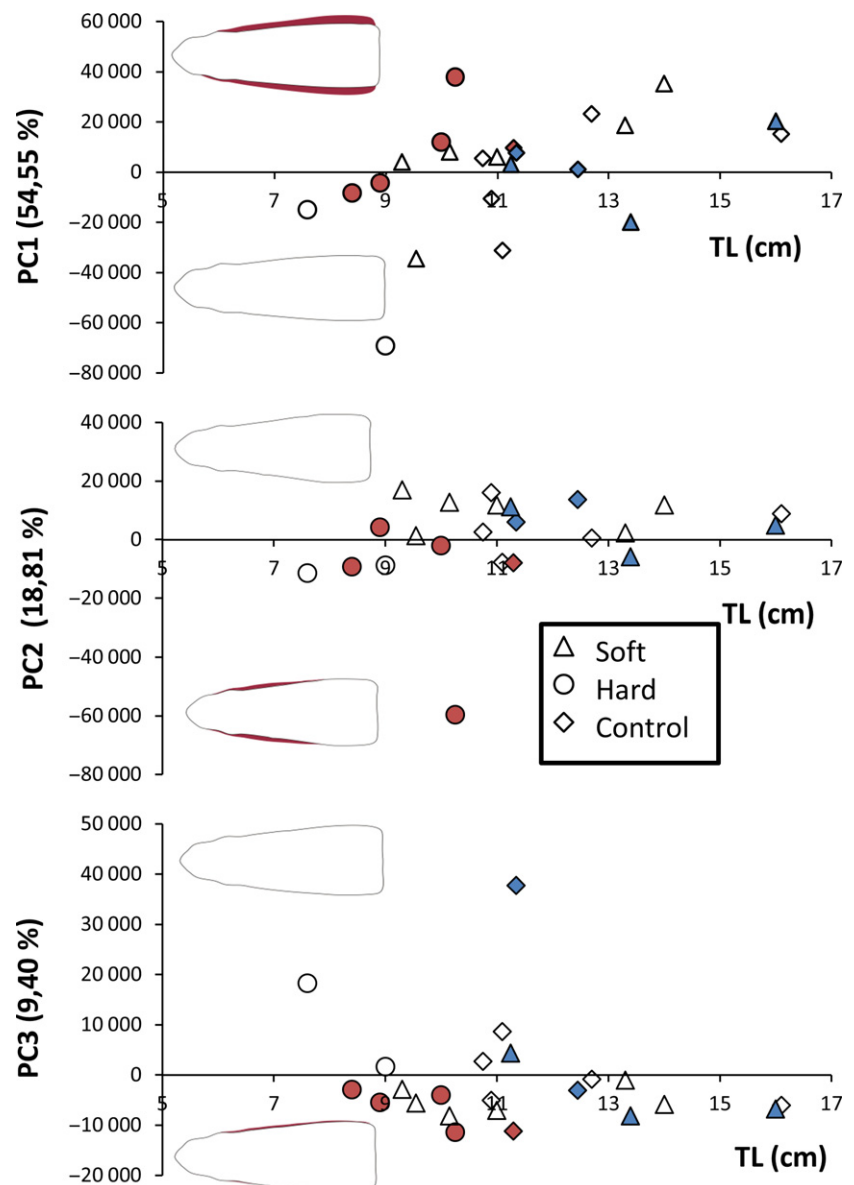

Fig. 2 Results of the shape analysis on elver eels (adapted from De Meyer et al. 2016), used for the selection of five broad-headed (red) and five narrow-headed elvers (blue) to be used in the current study. The graphs display the relation between the PC-scores of PC1–PC3 and total length (TL) of the specimens.

the elver eels could not be determined since these eels were still smaller than 20 cm, with sexual differentiation only becoming apparent in eels larger than 20 cm (Tesch, 2003). The sex of the selected yellow eels was determined by dissection and investigation of the gonads. All the yellow eels were female.

μCT-scanning

The heads of the selected specimens were removed at the start of the pectoral fins and were μCT-scanned twice. First, the heads were scanned untreated to visualize bone tissue. A second μCT-scan took place after the heads were treated with phosphomolybdic acid (2.5% solution for 14 days), which stains soft tissues (Metscher, 2009). Heads of the elver and yellow samples were scanned separately at the Centre for X-ray Tomography at Ghent University (UGCT) with the HECTOR μCT-scanner, built and developed in collaboration with the company X-Ray Engineering (www.xre.be). For the elver eels, the following set-up was used: 90-kV tube voltage and 2001 projections over 360°. The pixel pitch of the detector was 200 μm, with the reconstructed voxel sizes of the different specimens varying between 9.99 and 11.00 μm. For the yellow eels, 140-kV tube voltage was used and the number of projections over 360° varied between 1801 and 2401. The pixel pitch of the detector was again 200 μm, with the reconstructed voxel sizes of the different specimens varying between 29.99 and 45.00 μm. The μCT-data of the first scan was then processed to generate 3D-reconstructions of all the cranial bones, using AMIRA 5.5.0 (Visage Imaging, San Diego, CA, USA). The data of the second μCT-scan were used to make 3D-reconstructions of the different cranial muscles.

Morphological analysis

The skeletal 3D-reconstructions were used for two purposes. First, these reconstructions were used to describe how the skull develops from the elver to the yellow eel stage. Secondly, several measurements were taken on the skull to describe morphological differences between narrow- and broad-headed eels from the elver and yellow eel stages (Fig. 3). The 3D-reconstructions of the muscles were used to determine muscle volume and length, their origin and insertion, tendon length and its physiological cross-sectional area (PCSA), which are all used for morphological analysis and/or as input for the bite model. Nomenclature of the muscles follows Winterbottom (1973). When applicable, the skull and muscle measurements were calculated by averaging the measurements of the left and right side of the head, as eels were considered bilaterally symmetric. For the bite force model, the pennation angle and fiber length also need to be determined. Therefore, after μCT-scanning, the heads of the yellow eels were dissected and pictures were taken of the bipennate adductor mandibulae A1 muscle bundle with an Olympus SZX-ILL B200 to determine the pennation angle. For this, the angle was measured between the central tendon of the muscle and 10 individual muscle fibers and the pennation angle was then determined as the average of these angles (Supporting Information Fig. S1). Afterwards, the A1, A2 and A3 muscle bundles were removed from the head and immersed in a 30% HNO₃ solution for 48 h to isolate individual muscle fibers (Loeb & Gans, 1986). These fibers were then photographed using the Olympus SZX-ILL B200. The pennation angle and the length of 10 fibers per muscle bundle were measured using ImageJ. Afterwards, the average length of these muscle fibers was determined for each muscle bundle. The heads of the elver

eels were too small for proper dissection and were therefore not dissected.

Bite model

A static bite model was used to calculate bite forces at two positions along the lower jaw: a proximal bite point at the most posterior tooth, and a distal bite point at the most anterior tooth. Bite forces were calculated for the three muscle bundles of the adductor mandibulae complex: the large, lateral A1 muscle bundle and the two smaller, medial A2 and A3 muscle bundles. The lower jaw was assumed to form a single rigid body that can rotate about an axis through the left and right jaw joints. Mouth-closing torque about this axis was generated by the three different adductor mandibulae bundles (A1–A3) on each side of the head. The bipennate muscle-tendon model from van Leeuwen (1992) was used to calculate the muscle forces causing this torque. The 3D-geometry of this mechanical system and the muscle model was written in MATLAB SIMULINK version R2013b (8.2.0.701) using the SimMechanics toolbox (First Generation).

The dynamic model of a muscle–tendon complex with a bipennate muscle architecture by van Leeuwen (1992) applied to an isometric contraction at full, fused tetanus (i.e. stimulation pulses causing constant muscle force production) activation calculates muscle-tendon force F_{mtc} as:

$$F_{mtc} = (F_{cb0} \times \sigma_{miso} \times A_{f0} \times + F_{pas1} + F_{pas2}) \times \cos \alpha \quad (1)$$

where F_{cb0} is a normalized factor for cross-bridge force under isometric conditions and full activation to account for the force–length relationship (1 = optimum fiber length), σ_{miso} the maximal isometric stress of the muscle fibers at optimal length, A_{f0} is the physiological cross-sectional area (muscle volume V_m divided by fiber length at rest L_{f0}), F_{pas1} the passive force at short fiber lengths, resisting the cross-bridge force, and F_{pas2} the passive force above optimum fiber length, acting in parallel with the cross-bridge forces and α the pennation angle.

Bite forces were calculated at gape angle intervals of 10°, starting with the fish in resting position with an approximately closed mouth (i.e. how they were CT-scanned) and subsequently increasing the gape angle up to 40°. When the muscle is activated, the tendon is stretched, the muscle fibers rotate (i.e. pennation angle increases) and shorten. The relationships between the instantaneous length of the muscle-tendon complex, tendon length, muscle tendon force (F_{mtc}), fiber length and the angle of pennation, as described in equations 7 and 8 (and accompanying text) in van Leeuwen (1992), are used. In contrast to van Leeuwen (1992), we used a linear stress–strain relationship for the tendons and tendinous sheets of the muscle. We used a typical Young's modulus for tendon stiffness in our model (1 GPa; Alexander, 2002; Ker, 2007). As the contracting fibers become shorter than their resting length (i.e. the assumed position of optimal filament overlap in the sarcomeres; set at 10° gape angle), the initial force-length factors ($F_{cb0} = 1$, $F_{pas1} = F_{pas2} = 0$) may change due to stretching of the tendon.

For the bite force model, we assumed that the eel jaw muscles consist of white muscle fibers, as previous studies indicated that jaw muscles in fish mainly or solely consist of this fiber type (Baldwin et al. 1991; Maie et al. 2011). Furthermore, white muscles are used in other studies calculating theoretical bite force as well (Westneat,
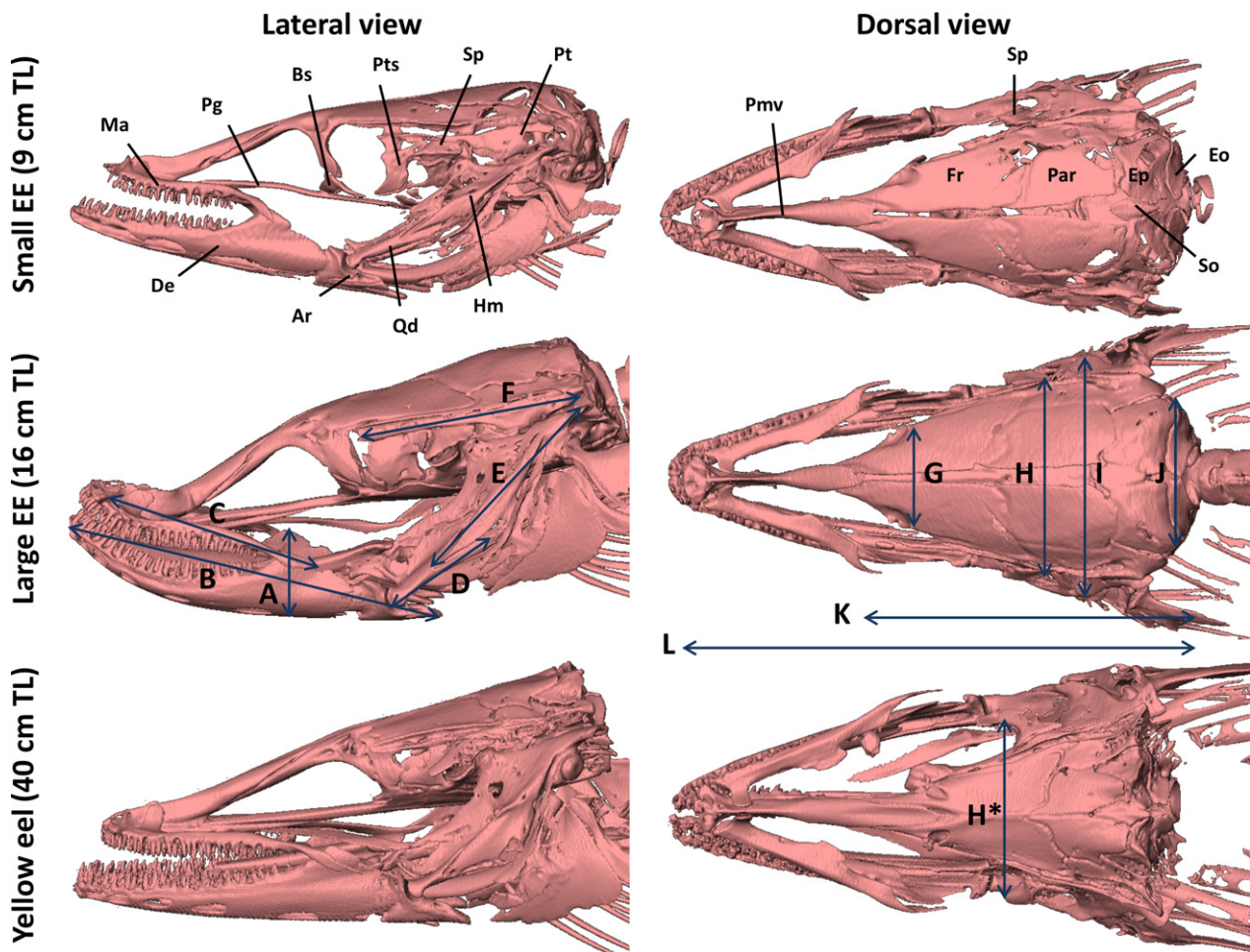
Fig. 3 3D-reconstruction of the skull of two elvers (EE) and one yellow eel in lateral and dorsal view, with indication of the most important bones. The snout of the large elver eel is slightly deformed because it was compressed in a small Eeppendorf tube for μCT-scanning. Ar, articulare; Bs, basisphenoid; De, dentary; Eo, exoccipital; Ep, epiotic; Fr, frontal; Hm, hyomandibula; Ma, maxilla; Par, parietal; Pg, pterygoid; Pmv, premaxillo-vomer complex; Pt, pterotic; Pts, pterosphenoid; Qd, quadrate; So, supraoccipital; Sp, sphenotic. Descriptions of the measurements are given in Table 1.

2003; Mara et al. 2009). A normalized force-length relationship (F_{cbo} being a function of instantaneous fiber length divided by optimum fiber length) was used based on a set of variables that describe the sarcomere ultrastructure as modeled by van Leeuwen in equations 2a to 2d of his article (van Leeuwen, 1991). We used the values for *Rana temporaria* (Linnaeus, 1758) tibialis muscles ($l_{myo} = 1.6$ μm, $l_{act} = 2.0$ μm, $l_z = 0.06$ μm, $l_{bz} = 0.15$ μm, $l_{min} = 0.5$ μm, $D_{act} = 0.68$, $D_{myo} = 1.9$; see van Leeuwen, 1991 for an explanation of these variables) as a representative of a vertebrate's white muscle used for fast and forceful actions. Since the simulations showed that F_{cbo} varied between 0.85 (at the ascending limb of the force–velocity relationship) and 1, passive, parallel elasticity forces F_{pas1} and F_{pas2} will not occur (van Leeuwen, 1991) and were thus zero in our model. Maximal isometric muscle stress σ_{miso} was set to 25 N cm^{-2}, as this value is commonly used for fast, glycolytic fibers (Herrel et al. 2008; Davis et al. 2010) and also falls within the range of values measured for the adductor mandibulae of teleost fishes (20.3 ± 8.7 N cm^{-2} in *Clarias gariepinus* Burchell, 1822; mean ± SD; Van Wassenbergh et al. 2007). This value was assumed to be equal for all specimens in our sample.

All the aforementioned muscular measurements of the 3D-reconstructions were used for the bite model. Volumes V_m and total muscle lengths of the three different muscles were calculated based on the 3D-reconstructions. The reported muscle volumes were calculated by averaging the muscle volumes of the left and right side of the head. For the yellow eels, the measured pennation angle and muscle fiber lengths were used, which are important determinants of bite force. The larger the pennation angle is, the more muscle fibers that can be packed in parallel in a muscle, which allows the generation of higher bite forces. In addition, fiber length is related to pennation angle, with a larger pennation angle being associated with shorter muscle fibers. In addition, a muscle consisting of a high number of short fibers will be able to generate a higher bite force than a muscle of similar volume with a lower number of long muscle fibers (Gans, 1982; Otten, 1998). For the elver eels, the pennation angle of the A1 and the fiber lengths of the different muscle bundles could not be determined. Therefore, 41.1°, the average pennation angle in yellow eels, was used (Goethals, 2015). Similarly, fiber length was estimated as one-third of the total muscle length for A1 and half of the total muscle length for A2 and A3, as

observed in yellow eels (Goethals, 2015). Finally, we collected 3D-coordinates of the insertion and origin of A1–A3, the left and right jaw joint, the tip of the most anterior and posterior tooth, and the anterior tip of the lower jaw. Subsequently, we translated and rotated these 3D-coordinates such that all reconstructed skulls were oriented in the same direction, with the jaw joints having the coordinates (0, 0, z) and the tip of the lower jaw (x, 0, 0). Finally, these coordinates together with the above-mentioned muscle model were then used to calculate the maximum bite forces of the different specimens. Maximum bite forces were always obtained at a gape angle of 10°, which corresponds to the situation in which the fiber lengths were optimal for active muscle force production ($F_{cbo} = 1$). Only these bite forces were used for further analysis.

Statistical analysis

The different skull measurements were corrected for total body length (TL). To correct muscle volume for TL, we calculated the cube root of each muscle volume and divided this cube root by TL. Finally, to correct bite force (BF) for body size, we calculated BF/TL^2 (TL expressed in mm) for each specimen. We then performed a non-parametric t-test in PAST (10 000 replicates) to find significant differences in skull measurements, muscle volume and bite force between the two phenotypes. However, since the sample sizes are small, the statistical analyses are less reliable. Because of this, we only provide the obtained P-values, while mainly focusing on the descriptive work.

To determine whether the dimorphism becomes more pronounced during the eel's ontogeny, we calculated the mean of each size-corrected skull measurement and muscle volume of broad-headed and narrow-headed elver and yellow eels. We then calculated the mean(broad-head)/mean(narrow-head) ratio of these measurement in the elver and yellow eel stage (referred to as the BH/NH ratio below) and compared these between both stages. In addition, we calculated and compared the variance of each measurement between both life stages.

Results

Morphological analysis: osteology

During the elver eel stage, the skull is not yet completely developed. In the smallest elvers (8–9 cm), the neurocranium is not yet completely ossified, leaving fontanels between the different bones (Fig. 3). Although most bones are already present at the preceding glass eel stage, two new bones are starting to develop when the eels become elver eels, namely, the supraoccipital and sphenotic. In addition, the pterosphenoid and basisphenoid, which are already present but still very small in glass eels, increase in size. In the largest elvers, the neurocranium is almost completely ossified. The pterotic, which is very prominent in glass eels and the smallest elvers, starts to flatten dorsoventrally (Fig. 3). Fontanels are still present between the prootic, pterosphenoid and basisphenoid in the largest elver eels. In the subsequent yellow eel stage, however, the bones are connected to each other by sutures and no fontanels remain. The pterotic is strongly flattened and the rostro-lateral side of the braincase is mainly taken up by the

fully ossified pterosphenoid and basisphenoid. Because of the differences in skull morphology between elvers and yellow eels, the skull width measurement between the pterotic bulbs in elvers was replaced by a skull width measured between the anterior end of the sphenotic bones in yellow eels (Table 1, Fig. 3).

After correcting the measurements for size, we observed that broad-headed and narrow-heads share the same characteristics across the elver and the yellow eel stage. Broad-heads in both life stages exhibit a longer skull. Accordingly, the pterotic, hyomandibula, quadrate and both the upper and lower jaws are longer in broad-headed eels than in narrow-headed ones. In addition, broad-headed eels are characterized by a relatively broader skull and a taller coronoid (Table 1). Unexpectedly, we observed that both the BH/NH ratio and the variance of the skull measurements are all lower in yellow eels than in elver eels (Table 1), suggesting that the skeletal differences are more pronounced in the elver eel stage than in the yellow eel stage.

Morphological analysis: myology

Whereas there are a lot of changes in skeletal morphology between the elver and the subsequent yellow eel stage, no major changes take place in the muscular morphology. The origin and insertion of the muscles is similar in both the different phenotypes and the different stages. The adductor mandibulae complex is the largest cranial muscle and consists of three subdivisions: A1, A2 and A3. The large, lateral A1 muscle bundle is the only muscle bundle that undergoes striking changes during development. Whereas it only covers the lateral side of the neurocranium in the glass eel stage, it also starts to cover the dorsal surface in the elver eel stage. In the yellow eel stage, the left and right A1 muscle bundles are hypertrophied such that they cover the complete dorsal surface, touching each other at the midline (Fig. 4). This muscle bundle originates ventro-caudally from the hyomandibula and preopercle, and covers the dorso-lateral surface of the frontals, parietals, epiotics and pterotics. The A1 exhibits two tendons which unite anteriorly, inserting on the caudal edge of the coronoid process. The A2 lies medial to the A1, originating from the ventro-lateral surface of the frontals, the lateral surface of the basi- and pterosphenoid, and the anterior surface of the sphenotic. Similar to the A1, A2 inserts on the caudal margin of the coronoid process, as well as on the medial side of the dentary. Finally, the A3 has its origin on the lateral surface of the hyomandibula and quadrate and inserts with a long anterior tendon on the medial surface of the dentary.

The dilatator operculi (DO) originates from the latero-caudal surface of the pterotic and the caudal surface of the sphenotic, inserting on the lateral surface of the opercular dorsal process. The levator operculi (LO) covers almost the complete opercle. It originates from the ventro-caudal pterotic surface, with its fibers inserting on the dorsal edge

Table 1 Mean ± SD, the mean(Broad-head)/mean(Narrow-head) ratio (BH/NH) and variance (Var.) of the different size-corrected skull, muscle and bite force measurements. The letter in parentheses corresponds to the measurements in Fig. 2. The size-corrected skull measurements were calculated by dividing the measurement by Total length. The size-corrected muscle volumes were calculated by taking the cube root of the muscle volumes and dividing these by TL. Finally, the size-corrected bite forces (BF) were calculated as BF/TL^2 (N mm^{-2}). The values of the size-corrected bite forces are expressed as mean ± SD ($\times 10^{-6}$). The given P-values are taken from a permutation test.

	Elver eel					Yellow eel				
	Mean ± SD ($\times 10^{-3}$)					Mean ± SD ($\times 10^{-3}$)				
	NH	BH	P	Var.	BH/NH	NH	BH	P	Var.	BH/NH
Skull										
Height coronoid (A)	8.3 ± 0.3	10.1 ± 1.0	0.005	1.2	1.22	11.2 ± 0.1	11.2 ± 0.6	0.10	0.9	1.14
Length lower jaw (B)	45.8 ± 0.6	51.6 ± 5.9	0.06	5.0	1.13	48.4 ± 1.7	52.7 ± 1.4	0.20	3.2	1.09
Length upper jaw (C)	27.2 ± 1.5	29.1 ± 3.6	0.33	2.9	1.07	30.3 ± 2.2	34.0 ± 1.5	0.20	2.6	1.12
Length quadrate (D)	15.8 ± 0.7	16.1 ± 1.8	0.72	1.4	1.02	14.8 ± 1.4	17.1 ± 1.6	0.18	1.9	1.16
Length hyomandibula (E)	26.3 ± 0.8	28.8 ± 4.5	0.27	3.3	1.09	26.0 ± 0.8	30.1 ± 2.2	0.10	2.6	1.15
Length pterotic (F)	24.8 ± 0.9	29.2 ± 2.6	0.02	3.0	1.18	29.4 ± 1.7	31.1 ± 1.2	0.13	1.6	1.06
SW pterotic (G)	34.9 ± 3.6	43.0 ± 2.8	0.007	5.2	1.23	9.8 ± 0.8	10.8 ± 1.4	0.34	1.1	1.11
SW bulb (H)	24.8 ± 0.6	28.8 ± 2.1	0.009	–	–	–	–	–	–	–
SW spenotic anterior (H*)	–	–	–	–	–	24.8 ± 1.2	26.7 ± 1.4	0.31	–	–
SW sphenotic posterior (I)	23.5 ± 0.6	27.1 ± 2.1	0.01	2.4	1.15	20.7 ± 0.4	21.8 ± 0.9	0.10	0.9	1.05
Caudal SW (J)	18.3 ± 0.1	21.8 ± 1.8	0.01	2.3	1.19	25.7 ± 0.6	27.4 ± 0.7	0.04	1.1	1.06
Length neurocranium (K)	37.1 ± 1.2	42.6 ± 3.6	0.02	7.1	1.16	38.8 ± 3.4	42.6 ± 0.6	0.13	2.6	1.06
Length skull (L)	64.8 ± 2.6	75.2 ± 5.9	0.04	3.9	1.15	61.3 ± 2.0	64.7 ± 2.0	0.10	3.0	1.10
Muscle										
A1	13.0 ± 1.3	13.5 ± 1.2	0.49	1198	1.04	14.7 ± 0.6	18.2 ± 0.3	< 0.01	1937	1.23
A2	6.1 ± 0.6	6.7 ± 0.8	0.21	728	1.10	6.3 ± 0.4	7.8 ± 0.5	< 0.01	921	1.24
A3	4.3 ± 0.2	4.7 ± 0.4	0.13	380	1.09	5.0 ± 0.3	5.7 ± 0.5	0.17	562	1.15
DO	4.4 ± 0.3	4.4 ± 0.4	0.98	308	1.00	4.6 ± 0.1	5.3 ± 0.1	< 0.01	372	1.15
LO	6.4 ± 0.3	6.4 ± 1.0	0.98	682	1.00	8.1 ± 0.5	9.3 ± 0.5	0.08	800	1.15
AO	4.0 ± 0.3	4.7 ± 1.1	0.17	–	–	–	–	–	–	–
LAP	5.9 ± 0.4	6.5 ± 0.7	0.14	–	–	–	–	–	–	–
AAP	6.4 ± 0.2	7.2 ± 0.4	0.02	–	–	–	–	–	–	–
PH	6.4 ± 0.4	7.2 ± 0.3	0.02	522	1.11	7.2 ± 0.3	8.3 ± 0.4	< 0.01	686	1.16
Bite force										
Proximal	0.81 ± 0.15	0.80 ± 0.39	0.96	–	–	2.44 ± 0.99	7.95 ± 2.33	< 0.01	–	–
Distal	0.26 ± 0.08	0.31 ± 0.11	0.43	–	–	0.31 ± 0.15	0.87 ± 0.28	< 0.01	–	–

and lateral surface of the opercle. Finally, the adductor operculi (AO) stretches from the lateral exoccipital surface and the dorso-lateral surface of the basioccipital to the medial surface of the opercle.

The triangular, medially located levator arcus palatini (LAP) originates from the outer and ventral surface of the sphenotic and inserts on the pterygoid, quadrate and hyomandibula. Most fibers of the adductor arcus palatini (AAP) originate from the parasphenoid, but some fibers also from the prootic. It inserts on the dorsal edge and the medio-caudal surface of the pterygoid, but mainly on the quadrate and hyomandibula. Finally, the protractor hyoidei (PH) originates from the medial surface and inserts on the lateral surface of the posterior ceratohyal.

The broad-headed elvers are significantly smaller in total length (mean ± SD: 97.8 ± 11.5 mm; P = 0.02) than the narrow-headed ones (129.2 ± 19.3 mm) in our study. Because of this size difference, we need to correct for body size. After size correction, we observe that broad-headed elvers exhibit larger muscles compared with narrow-heads, with the exception of DO and LO, which are equal in size in both phenotypes (Table 1).

Whereas in the elver eel stage, broad-heads are smaller than narrow-heads in total length, the opposite is the case in the yellow eel stage. The broad-headed yellow eels are significantly larger (542.3 ± 44.8 mm; P < 0.01) than the narrow-headed ones (382.0 ± 24.3 mm). Two weeks of staining was insufficient for two broad-headed yellow eels and consequently no reconstructions could be made for the muscles AO, AAP and LAP in these specimens. These three muscles are therefore not used for further analysis. After size correction, we found that also here, all muscles (A1, A2, A3 and PH) are larger in broad-headed yellow eels than in narrow-headed ones (Table 1). Interestingly, DO and LO, which did not differ in size in the elver eel stage, are larger in broad-headed yellow eels than narrow-headed ones.
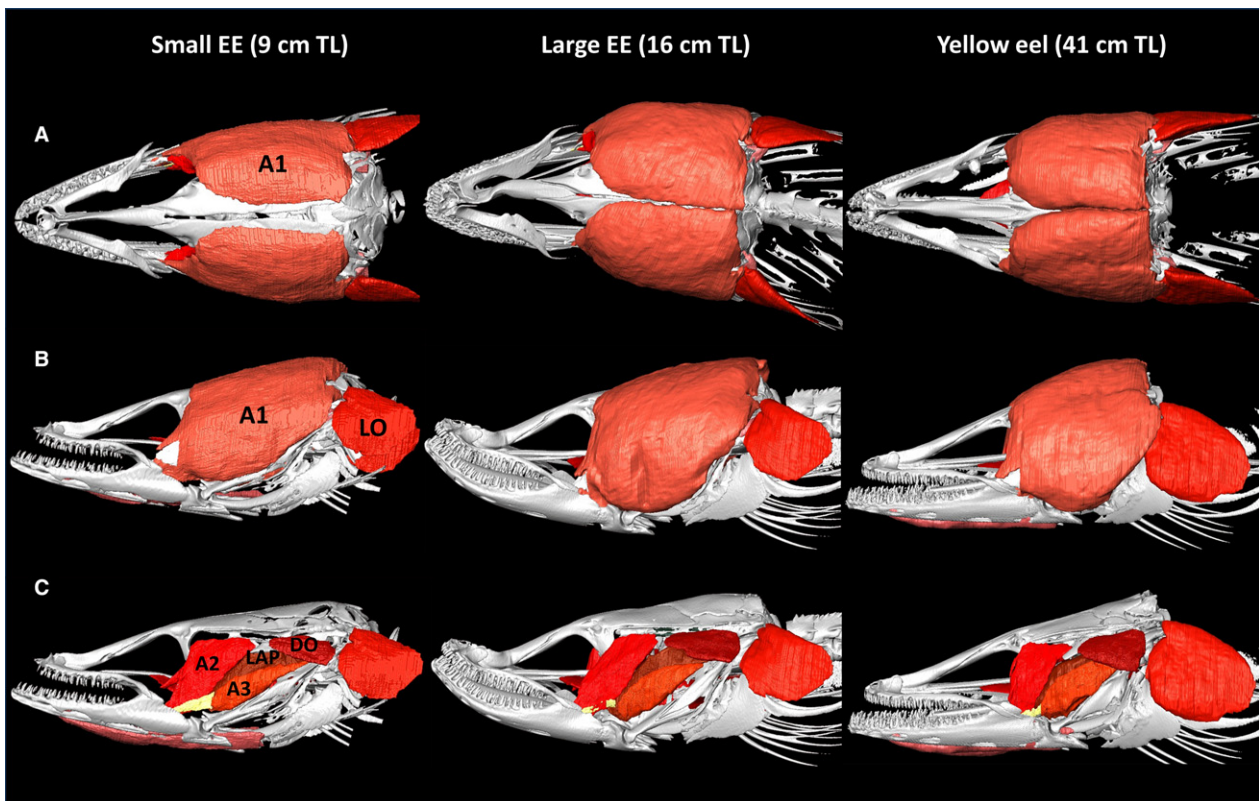
Fig. 4 3D-reconstruction of the cranial muscles of two elvers (EE) and one yellow eel, with indication of the most important muscles. (A) Dorsal view on the skull and A1. (B) Lateral view of the different muscles. (C) Lateral view of the different muscles after removal of A1. A1–A3: adductor mandibulae 1–3. DO, dilatator operculi; LAP, levator arcus palatini; LO, levator operculi.

In contrast with the skull measurements, we observe that both the BH/NH ratio and the variance of the muscle volumes increase from elver to yellow eels. This suggests that the differences in muscle volume between the two phenotypes become more pronounced during the eel's ontogeny.

Bite force

The bite force predictions indicate that most of the bite force is generated by the large A1 muscle bundle in both phenotypes and in both stages, with A2 and especially A3 adding only little to the total bite force (Fig. 5). The bite forces generated at the distal bite point are generally only half of those generated at the proximal bite point in both life stages (Fig. 5). In the elver eel stage, the total predicted bite force ranged between 0.02 and 0.17 N in broad-heads at the proximal bite point. For the narrow-headed elvers, proximal bite force ranged between 0.12 and 0.26 N. While the absolute bite forces are higher in narrow-headed elvers, the size-corrected bite forces are similar at the proximal and higher at the distal bite point in broad-headed elvers (Table 1), even when taking into account that the smallest broad-head has a very low bite force in comparison with the other eels. Furthermore, we observe that broad-headed

elvers of similar size as or smaller than certain narrow-heads are capable of generating higher bite forces (Fig. 5).

In the yellow eel stage, we found that broad-heads are capable of generating much higher bite forces (min–max: 16.3–36.3 N) than narrow-heads (min–max: 2.8–6.9 N). These differences could be due to the strong differences in size. However, we also found that the size-corrected bite forces are higher in broad-headed yellow eels than in narrow-headed ones (Table 1). As such, our bite force predictions indicate that broad-headed eels are capable of generating higher bite forces than narrow-heads in both life stages.

Discussion

With this study, we wanted to identify the cranial musculoskeletal features characteristic for broad- and narrow-heads in two different life stages of the European eel, namely the elver and the subsequent yellow eel stage. We found that broader heads are associated with larger muscles in both stages, whereas no obvious changes in fiber orientation are observed between the elver eel and yellow eel stage. In addition, we observed that broader heads are associated with relatively broader and longer skulls, and elongated upper and lower jaws accompanied by a taller
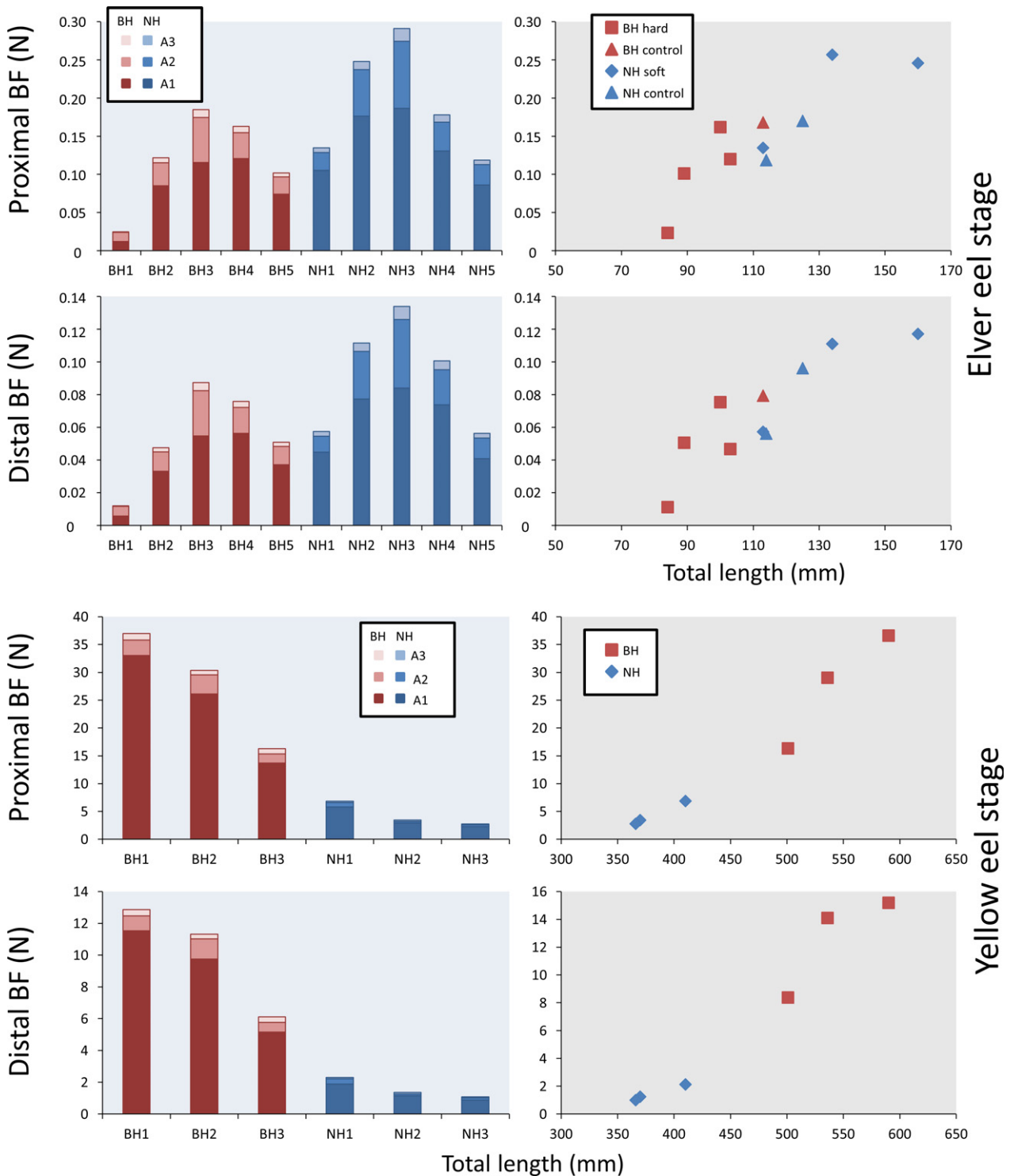
Fig. 5 Graphs showing the maximum proximal and distal bite force generated by each muscle bundle for each specimen (left) and the relation between the total length of the specimens and the bite force they can generate.

coronoid. The same musculoskeletal differences were observed in the glass eel stage, the stage preceding the elver eel stage (De Meyer et al. 2018). As such, we can conclude that broad-heads in different life stages share the same modifications in the musculoskeletal system of the feeding apparatus as do narrow-heads. This could affect their feeding performance, corresponding to the observed differences in diet (Lammens & Visser, 1989).

Muscle hypertrophy, for example, is a common way to increase bite force (Herrel et al. 2007b). This is the case in air-breathing catfishes (Herrel et al. 2002), several lizard species (Verwaijen et al. 2002; Herrel et al. 2007a), finches (van der Meij & Bout, 2004) and even humans (Raadsheer et al. 1999). Consequently, the larger jaw muscles of broad-headed eels can have a positive impact on bite force, allowing more efficient consumption of harder prey. The relatively broader and longer neurocranium of broad-headed elver and yellow eels could then be a way to provide an increased insertion surface for the larger A1 muscle bundle. In addition, the taller coronoid process of broad-heads not only provides a larger attachment surface for the jaw-closing muscles, extending the lever arm also increases the mechanical advantage (Popowics & Herring, 2006). Both these factors can be related to higher bite forces (Cabuy et al. 1999; Herrel et al. 2002). Simultaneously, the larger mechanical advantage of broad-heads could allow these eels to generate relatively higher bite forces at higher gape angles compared with narrow-heads, which can be beneficial when dealing with larger prey items (Santana et al. 2010).

While broad-heads exhibit several characteristics that could be beneficial for increasing bite force, it is known that European eels can also spin along their long axis to tear off smaller pieces of large, hard prey items which, meanwhile, are kept in the mouth (Helfman & Winkelman, 1991). The larger jaw muscles of broad-heads may therefore also improve holding grip and preventing dislodgement of the lower jaws during spinning (De Schepper, 2007). Furthermore, broad-heads exhibit longer upper and lower jaws; this, associated with a longer tooth row, can improve keeping a tight grip on prey items during spinning.

The above-described differences in the musculoskeletal system between broad- and narrow-heads can have an impact on their the feeding performance, i.e. their ability to handle and process prey (Wainwright, 1988, 1991). By analyzing the magnitude and differences in bite force between broad- and narrow-heads, it is possible to link the variation in the feeding apparatus to feeding performance. In addition, as it allows the determination of potential prey items, differences in bite force could explain why broad- and narrow-heads consume different diets (Huber & Motta, 2004). Interestingly, after correcting the bite forces for body size, no strong differences in bite force are observed between broad- and narrow-heads in the elver eel stage, whereas considerable differences were found in the yellow eel stage. Our bite force predictions, however, still indicate that broad-headed eels should be able to generate higher bite forces in both life stages.

The more pronounced differences in bite force between broad- and narrow-heads in the yellow eel stage could allow yellow eel populations to consume a broader range of prey. The predicted bite forces of the broad-headed yellow eels, for example, should be large enough to deal with small fish such as gobies and smaller crustaceans (Huber, 2006; Habegger et al. 2011; Marshall et al. 2012), whereas this will be more difficult for the narrow-headed ones. Furthermore, the predicted bite force of the yellow eels suggests that European eels are opportunistic feeders, rather than being strictly durophagous or suction-feeding fishes. The bite forces of broad-headed yellow eels are relatively low compared with strictly durophagous fishes (Mara et al. 2009), but high compared with suction-feeding fish similar in size (Huber & Motta, 2004). Elver eels, on the other hand, are smaller and therefore should have a more size-restricted diet. The predicted maximum bite force of the elver eels is high enough to feed on small crustaceans such as *Gammarus fossarum* (Koch, 1836) but not on fishes and larger crustaceans (Huber, 2006; Habegger et al. 2011; Błońska et al. 2015). So, even though broad-headed elvers should be more efficient than narrow-headed ones in consuming these smaller crustaceans, the differences in hardness and size of the consumed prey should be lower in this stage.

In this study, we also wanted to investigate whether the musculoskeletal differences associated with broad- and narrow-headedness become more pronounced during ontogeny. The differences in muscle volume between the two phenotypes are equally pronounced in the glass and elver eel stage but become more pronounced in the yellow eel stage. The differences in skeletal morphology, on the other hand, are least pronounced in the glass eels (De Meyer et al. 2018) and largest in elvers, for which several explanations can be given.

A first possibility is that the sample size of the yellow eels was just too low to find large differences in skeletal morphology. A second explanation relates to the eel's ecology and development. Most elver eels of this study were fed a strict hard or soft diet, requiring biting or spinning behavior and suction-feeding, respectively. As such, the differences in feeding behavior could be associated with large differences in the mechanical loading exerted on the skull between the two phenotypes. As elver eels are osteologically and myologically still not fully developed, they are more prone than yellow eels to morphological changes in response to diet (Hinton & McNamara, 1984; Wund et al. 2008), which can lead to pronounced changes in the skull morphology. On the other hand, the yellow eels in this study were wild-caught and can be considered to exhibit a less strict diet (Tesch, 2003). The skulls of the yellow eels were possibly mechanically stimulated less extensively during development than those of the elver eels in this study, which could explain the more pronounced skeletal differences in elver eels compared with yellow eels (Witten & Hall, 2015).

However, the opposite scenario could apply to the muscles. Broad-headed yellow eels can feed on relatively larger and harder prey compared with broad-headed elvers. The consumption of these relatively harder and larger prey could consequently stimulate muscle activity more in broad-

headed yellow eels, inducing more extensive muscle enlargement (Chromiak & Antonio, 2006).

A third and final explanation for the more pronounced muscular and less pronounced skeletal differences in yellow eels might be related to spatial constraints in the cranial musculoskeletal system. Space taken up by jaw adductors, for example, leaves less space for the central nervous system when the total skull volume remains constant (Herrel et al. 2007b). Finally, it is possible that a combination of the above explanations explains our observations.

The expression of a dimorphic head shape in different life stages has the benefit that it can strongly decrease intraspecific trophic competition. Broad-headed elvers are better suited to feed on small crustaceans such as *Gammarus* sp., whereas narrow-headed elvers are more likely stick to small benthic invertebrates such as chironomid larvae. Additionally, the decreased gape limitation of growing eels allows a gradually increased consumption of snails, molluscs and fish (Tesch, 2003). This lowers the competition between the elver and yellow eels for the same prey. Simultaneously, also within the yellow eel stage, broad-headed phenotypes are more capable of handling, and therefore also more likely to eat, harder, larger prey items compared with their narrow-headed counterparts (Sivertsen, 1938; Lammens & Visser, 1989). The potential to consume different prey items in a single life stage, but also during different life stages, can strongly decrease the competitive pressure for food (Schoener, 1974; Papastamatiou et al. 2006; Espinoza et al. 2012). Considering that European eels require a fat percentage of at least 12% to migrate successfully 6000 km towards the spawning areas in the Sargasso Sea (Van den Thillart et al. 2007), decreasing intraspecific competition by consuming different prey items can be very important for eel survival.

In conclusion, the musculoskeletal morphology of the feeding apparatus of the European eel is clearly linked to its bite performance and is therefore expected to be linked to their trophic ecology (Arnold, 1983; Wainwright & Reilly, 1994). Broad-heads scaled to a similar body size as narrow-heads exhibit enlarged adductor mandibulae, a broader skull and longer jaws with a taller coronoid process. All these traits are expected to improve bite performance and/or facilitate spinning behavior for dealing with harder, larger prey. Additionally, larger eels can consume larger prey due to their wider gape, which can result in dietary shifts during the eels' development. As such, intraspecific competition in the European eels could be decreased both between different life stages and between different phenotypes in each life stage.

Acknowledgements

Author contributions

J. De Meyer was responsible for the 3D-reconstructions, analysis of the data and writing of the manuscript. T. Goethals was responsible for the dissections of the yellow eels and the determination of the A1 pennation angles and the fiber lengths of the jaw muscles. S. Van Wassenbergh developed the bite model and helped write the manuscript. T. Augustijns, J. Habraken, J. Hellemans & V. Vandewiele made preliminary 3D-reconstructions of the elver and yellow eels, which were finalized by J. De Meyer. J. Dhaene was responsible for the CT-scanning of the specimens. M. Bouilliart helped determine the correct input data for the bite model. D. Adriaens supervised the research and helped with writing the manuscript.

References

Alexander RM (2002) Tendon elasticity and muscle function. *Comparative Biochemistry and Physiology part A* **133**, 1001–1011.

Arnold SJ (1983) Morphology, performance and fitness. *Am Zool* **23**, 347–361.

Artero C, Koenig CC, Richard P, et al. (2015) Ontogenetic dietary and habitat shifts in goliath grouper *Epinephelus itajara* from French Guiana. *Endangered Species Res* **27**, 155–168.

Baldwin J, Davison W, Forser ME (1991) Anaerobic glycolysis in the dental plate retractor muscles of the New Zealand hagfish *Eptatretus cirrhatus* during feeding. *J Exp Biol* **260**, 295–301.

Bertin L (1956) *Eels: A Biological Study*. London: Cleaver-Hume Press, 192 pp.

Błońska D, Grabowska J, Kobak J, et al. (2015) Feeding preferences of an invasive Ponto-Caspian goby for native and non-native gammarid prey. *Freshw Biol* **60**, 2187–2195.

Bohórquez-Herrera J, Cruz-Escalona VH, Adams DC, et al. (2014) Feeding ecomorphology of seven demersal marine fish species in the Mexican Pacific Ocean. *Environ Biol Fishes* **98**, 1459–1473.

Cabuy E, Adriaens D, Verraes W, et al. (1999) Comparative study on the cranial morphology of *Gymnallabes typus* (Siluriformes: Clariidae) and their less anguilliform relatives, *Clariallabes melas* and *Clarias gariepinus*. *J Morphol* **240**, 169–194.

Chromiak JA, Antonio J (2006) Skeletal muscle plasticity. In: *Essentials of Sports Nutrition and Supplements* (eds Antonio J, Kalman D, Stout JR, Greenwood L, Willoughby DS, Haff GG). 21–52, Totowa: Springer Science.

Clifton KB, Motta PJ (1998) Feeding morphology, diet and ecomorphological relationships among five Caribbean labrids (Teleostei, Labridae). *Copeia* **1998**, 953–966.

Costalago D, Navarro J, Álvarez-Calleja I, et al. (2012) Ontogenetic and seasonal changes in the feeding habits and trophic levels of two small pelagic fish species. *Mar Ecol Prog Ser* **460**, 169–181.

Davis JL, Santana SE, Dumont ER, et al. (2010) Predicting bite force in mammals: two-dimensional versus three-dimensional lever models. *J Exp Biol* **213**, 1844–1851.

De Meyer J, Ide C, Belpaire C, et al. (2015) Head shape dimorphism in European glass eels (*Anguilla anguilla*). *Zoology* **118**, 413–423.

De Meyer J, Christiaens J, Adriaens D (2016) Diet-induced phenotypic plasticity in European eel (*Anguilla anguilla*). *J Exp Biol* **219**, 354–363.

De Meyer J, van Wassenbergh S, Bouilliart M, et al. (2018) Built to bite? Differences in cranial morpholology and bite performance between narrow- and broad-headed European glass eels. *J Morphol* **279**, 349–360.

De Schepper N (2007) *Evolutionary Morphology of Body Elongation in Teleosts: Aspects of Convergent Evolution*. PhD dissertation, Ghent University.

Espinoza M, Clarke TM, Villalobos-Rojas F, et al. (2012) Ontogenetic dietary shifts and feeding ecology of the rasptail skate *Raja velezi* and the brown smoothhound shark *Mustelus henlei* along the Pacific coast of Costa Rica, Central America. *J Fish Biol* **81**, 1578–1595.

Gans C (1982) Fiber architecture and muscle function. *Exerc Sport Sci Rev* **10**, 160–207.

Goethals T (2015) *Head shape dimorphism en European eels (Anguilla anguilla): Assessing myology and bite force in broadheads and narrowheads*. Master thesis, Ghent University. Ghent, Belgium. 29 pages.

Habegger ML, Motta PJ, Huber DR, et al. (2011) Feeding biomechanics in the Great Barracuda during ontogeny. *J Zool* **283**, 63–72.

Hahn NS, Cunha F (2005) Feeding and trophic ecomorphology of *Satanoperca pappaterra* (Pisces, Cichlidae) in the Manso reservoir, Mato Grosso State, Brazil. *Braz Arch Biol Technol* **48**, 1007–1012.

Helfman GS, Winkelman DL (1991) Energy trade-offs and foraging mode choice in American eels. *Ecology* **72**, 310–318.

Hernandez LP, Motta PJ (1997) Trophic consequences of differential performance: ontogeny of oral jaw-crushing performance in the sheepshead, *Archosargus probatocephalus* (Teleostei, Sparidae). *J Zool* **243**, 737–756.

Herrel A, O'Reilly JC (2006) Ontogenetic scaling of bite force in lizards and turtles. *Physiol Biochem Zool* **79**, 31–42.

Herrel A, Damme RV, Vanhooydonck B, et al. (2001a) The implications of bite performance for diet in two species of lacertid lizards. *Can J Zool* **79**, 662–670.

Herrel A, De Grauw E, Lemos-Espinal JA (2001b) Head shape and bite performance in Xenosaurid lizards. *J Exp Zool* **290**, 101–107.

Herrel A, Adriaens D, Verraes W, et al. (2002) Bite performance in clariid fishes with hypertrophied jaw adductors as deduced by bite modeling. *J Morphol* **253**, 196–205.

Herrel A, McBrayer LD, Larson PM (2007a) Functional basis for sexual differences in bite force in the lizard *Anolis carolinensis*. *Biol J Lin Soc* **91**, 111–119.

Herrel A, Schaerlaeken V, Meyers JJ, et al. (2007b) The evolution of cranial design and performance in squamates: consequences of skull-bone reduction on feeding behavior. *Integr Comp Biol* **47**, 107–117.

Herrel A, De Smet A, Aguirre LF, et al. (2008) Morphological and mechanical determinants of bite force in bats: do muscles matter? *J Exp Biol* **211**, 86–91.

Hinton RJ, McNamara JA (1984) Effect of age on the adaptive response of the adult temporomandibular joint. A study of induced protrusion in *Macaca mulatta*. *Angle Orthod* **54**, 154–162.

Huber DR (2006) *Cranial Biomechanics and Feeding Performance of Sharks*. PhD thesis, University of South Florida.

Huber DR, Motta PJ (2004) Comparative analysis of methods for determining bite force in the spiny dogfish, *Squalus acanthias*. *J Exp Zool A Comp Exp Biol* **301**, 26–37.

Ide C, De Schepper N, Christiaens J, et al. (2011) Bimodality in head shape in European eel. *J Zool* **285**, 230–238.

Iijama M (2017) Assessment of trophic ecomorphology in non-alligatoroid crocodylians and its adaptive and taxonomic implications. *J Anat* **231**, 192–211.

Ker R (2007) Mechanics of tendon, from an engineering perspective. *International Journal of Fatigue* **29**, 1001–1009.

Lammens EHRR, Visser JT (1989) Variability of mouth width in European eel, *Anguilla anguilla*, in relation to varying feeding conditions in three Dutch lakes. *Environ Biol Fishes* **26**, 63–75.

van Leeuwen JL (1991) Optimum power output and structural design of sarcomeres. *J Theor Biol* **149**, 229–256.

van Leeuwen JL (1992) Muscle funtion in locomotion. In: *Mechanics of Animal Locomotion* (ed. Alexander RM), pp. 191–250. Heidelberg: Springer-Verlag.

Loeb GE, Gans C (1986) *Electromyography for Experimentalists*. University of Chicago press.

Lopez-Darias M, Vanhooydonck B, Cornette R, et al. (2015) Sex-specific differences in ecomorphological relationships in lizards of the genus *Gallotia*. *Funct Ecol* **29**, 506–514.

Machado-Evangelista M, Esguícero ALH, Arcifa MS, et al. (2015) Diet and ecomorphology of *Leporinus reticulatus* (Characiformes: Anostomidae) from the upper Rio Juruena, MT, Brazil: ontogenetic shifts related to the feeding ecology. *Acta Amazon* **45**, 383–392.

Maie T, Meister AB, Leonard GJ, et al. (2011) Jaw muscle fiber type distribution in Hawaiian gobioid stream fishes: histochemical correlations with feeding ecology and behavior. *Zoology* **114**, 340–347.

Mara KR, Motta PJ, Huber DR (2009) Bite force and performance in the durophagous bonnethead shark, *Sphyrna tiburo*. *J Exp Zool A Ecol Genet Physiol* **313**, 95–105.

Marshall CD, Guzman A, Narazaki T, et al. (2012) The ontogenetic scaling of bite force and head size in Loggerhead Sea turtles (*Caretta caretta*): implications for durophagy in neritic, benthic habitats. *J Exp Biol* **215**, 4166–4174.

van der Meij MAA, Bout RG (2004) Scaling of jaw muscle size and maximal bite force in finches. *J Exp Biol* **207**, 2745–2753.

Metscher BD (2009) MicroCT for developmental biology: a versatile tool for high-contrast 3D imaging at histological resolutions. *Dev Dyn* **238**, 632–640.

Meyer A (1989) Cost of morphological specialization: feeding performance of the two morphs in the trophically polymorphic cichlid fish, *Cichlasoma citrinellum*. *Oecologia* **80**, 431–436.

Moriarty C (1973) Studies of the eel *Anguilla anguilla* in Ireland. 1. In the lakes of the Corrib system. *Ir Fish Investig A* **13**, 1–13.

Narayani S, Venu S, Arun KM, et al. (2015) Ecomorphology of the feeding characteristics in selected reef fishes from south Andamanislands: a preliminary study. *J Mar Biol Oceanogr* **4**, 2.

Norton SF, Brainerd EL (1993) Convergence in the feeding mechanics of ecomorhpologically similar species in the Centrarchidae and Cichlidae. *J Exp Biol* **176**, 11–29.

Otten E (1998) Concepts and models of functional architecture in skeletal muscles. *Exerc Sport Sci Rev* **16**, 89–137.

Papastamatiou YP, Wetherbee BM, Lowe CG, et al. (2006) Distribution and diet of four speciees of carcharhinid shark in the Hawaiian islands: evidence for resource partitioning and competitive exclusion. *Mar Ecol Prog Ser* **320**, 239–251.

Popowics TE, Herring SW (2006) Teeth, jaws and muscles in Mammalian mastication. In: *Feeding in Domestic Vertebrates: from Structure to Behavior* (ed. Bels VL), pp. 61–83. Wallingford: CABI Publishing.

Proman JM, Reynolds JD (2000) Differences in head shape of the European eel. *Fish Manage Ecol* **7**, 349–354.

Raadsheer MC, van Eijden TMGJ, van Ginkel FC, et al. (1999) Contribution of Jaw muscle and craniofacial morphology to human bite force magnitude. *J Dent Res* **78**, 31–42.

Riccialdelli L, Newsome SD, Dellabianca NA, et al. (2013) Ontogenetic diet shift in Commerson's dolphin (*Cephalorhynchus commersonii commersonii*) off Tierra del Fuego. *Polar Biol* **36**, 617–627.

Santana SE, Miller KE (2016) Extreme postnatal scaling in bat feeding performance: a view of ecomorphology from ontogenetic and macroevolutionary perspectives. *Integr Comp Biol* **56**, 459–468.

Santana SE, Dumont ER, Davis JL (2010) Mechanics of bite force production and its relationship to diet in bats. *Funct Ecol* **24**, 776–784.

Saunders MB, Barclay RMR (1992) Ecomorphology of insectivorous bats: a test of predictions using two morhpologically similar species. *Ecology* **73**, 1335–1345.

Schoener TW (1974) Resource partitioning in ecological communities. *Science* **185**, 27–39.

Sinha VRP, Jones JW (1967) On the food of the freshwater eels and their feeding relationship with the salmonids. *J Zool* **153**, 119–137.

Sivertsen E (1938) Undersøkelser over forholdet mellem spiss- og bredhodet ål og deres næring. *Fiskeridirek Skr* **5**, 1–22.

Tesch FW (2003) *The Eel*. Oxford: Blackwell Science.

Thurow F (1958) Untersuchungen über die spitz und breitköpfigen Varianten des Flussaales. *Arch Fischereiw* **9**, 79–97.

Van den Thillart GEEJM, Palstra AP, Van Ginneken VJT (2007) Stimulated migration of European silver eel: swim capacity and cost of transport. *J Mar Sci Technol* **15**(special issue), 1–16.

Van Wassenbergh S, Herrel A, James RS, et al. (2007) Scaling of contractile properties of catfish feeding muscles. *Journal of Experimental Biology* **210**, 1183–1193.

Verwaijen D, van Damme R, Herrel A (2002) Relationships between head size, bite force, prey handling efficiency and diet in two sympatric lacertid lizards. *Funct Ecol* **16**, 842–850.

Wainwright PC (1988) Morphology and ecology: functional basis of feeding constraints in Caribbean labrid fishes. *Ecology* **69**, 635–645.

Wainwright PC (1991) Ecomorphology: experimental functional anatomy for ecological problems. *Am Zool* **31**, 680–693.

Wainwright PC, Reilly SM (1994) *Introduction. Ecological Morphology: Integrative Organismal Biology*. Chicago: University of Chicago Press.

Webb PW (1984) Body form, locomotion and foraging in aquatic vertebrates. *Am Zool* **24**, 107–120.

Westneat MW (2003) A biomechanical model for analysis of muscle force, power output and lower jaw motion in fishes. *J Theor Biol* **223**, 269–281.

Wilga CD, Diniz SE, Steele P, et al. (2016) Ontogeny of feeding mechanics in smoothhound sharks: morphology and cartilage stiffness. *Integr Comp Biol* **56**, 442–448.

Winterbottom R (1973) A descriptive synonymy of the striated muscles of the Teleostei. *Proc Acad Natl Sci Philadelphia* **125**, 225–317.

Witten PE, Hall BK (2015) Teleost skeletal plasticity: modulation, adaptation, and remodelling. *Copeia* **103**, 727–739.

Wund MA, Baker JA, Clancy B, et al. (2008) A test of the 'flexible stem' model of evolution: ancestral plasticity, genetic accommodation, and morphological divergence in the three-spine stickleback radiation. *Am Nat* **172**, 449–462.

Wyckmans M, van Wassenbergh S, Adriaens D, et al. (2007) Size-related changes in cranial morphology affect diet in the catfish *Clariallabes longicauda*. *Biol J Linnean Soc* **92**, 323–334.

Supporting Information

Additional supporting information may be found online in the Supporting Information section at the end of the article:

Table S1. Origin of the different specimens used in this study. BH, broad-head; NH, narrow-head.

Fig. S1. Figure indicating how the pennation angle was determined for the bipennate adductor mandibulae A1 muscle bundle.